Expedited Neighbor Discovery in Directional Terahertz Communication Networks Enhanced by Antenna Side-Lobe Information

Qing Xia ⬤, *Member, IEEE*, and Josep Miquel Jornet ⬤, *Member, IEEE*

Abstract—Terahertz (THz)-band (0.1–10 THz) communication is envisioned as a key wireless technology of the next decade, able to support wireless Terabit-per-second links in 6G systems. THz communication exhibits an extremely large bandwidth (tens to hundreds of GHz) at the cost of a very high path loss ($>$100 dB for distances beyond a few meters). Therefore, highly directional antennas (DAs) are needed simultaneously in transmission and reception at all times to establish reliable communication links. The application of highly DAs introduces new challenges in the neighbor discovery process. In this paper, a time-efficient neighbor discovery protocol for THz-band communication networks is proposed. The protocol expedites the neighbor discovery process by leveraging the full antenna radiation pattern to detect a series of effective signals and map them to the universal signal patterns, which indicate the potential direction of the signal source. A mathematical framework is developed to compare the neighbor discovery protocols with and without the antenna side-lobes information in free space. The X60 testbed is utilized to validate the proposed neighbor discovery protocol. Furthermore, a feasibility analysis of the proposed protocol inside a bounded space (e.g., a square room) is conducted. Numerical results are presented to illustrate the performance improvements achieved by the proposed protocol when compared to the traditional neighbor discovery protocols with only main-lobe information.

Index Terms—Terahertz communications, neighbor discovery, 6G systems.

I. INTRODUCTION

THE way in which our society creates, shares and consumes information has lead to a drastic increase in wireless data traffic. Not only are there more devices connected to the internet, but wireless data rates are much higher too. Wireless data rates have grown 18-fold over the past 5 years [2], and are approaching the capacity of the wired communication systems. Following this trend, wireless Terabits-per-second (Tbps) links are expected to become a reality in the near future. In this context, Terahertz

(THz)-band (0.1–10 THz) communication is envisioned as a key technology to satisfy such very high data-rates [3], [4].

The THz band provides wireless communication with a remarkably large bandwidth (tens to hundreds of GHz). However, this advantage comes at the cost of a very high propagation loss [5], [6], which is mainly caused by the spreading loss and the molecular absorption loss. The latter defines multiple absorption lines whose strength and width increases with distance and effectively splits the THz band into multiple transmission windows. This very large bandwidth enables physical-layer data rates in the order of hundreds of Gbps or a few Tbps, even with low-complexity modulations [7].

Due to the limited power of THz transceivers, which ranges from tens of microWatts [8] to tens of milliWatts [9], highly Directional Antennas (DAs) are needed simultaneously in transmission and reception at all times to overcome the very high propagation loss. The application of highly DAs introduces new challenges when moving up in the protocol stack. For instance, synchronization at the link layer, relaying and routing at the network layer, and many others require knowledge of the neighboring nodes. Therefore, time-efficient neighbor discovery protocols are of critical importance.

The existing neighbor discovery protocols for lower frequency communication networks cannot be directly reused, because they do not capture the peculiarities of THz-band communication networks. Most of the existing solutions for the directional communication networks consider that one node in a communication link can temporarily operate with a quasi omnidirectional antenna while the other node utilizes the directional antenna [10]–[12]. Unfortunately, the two nodes need to be highly directional at all times to overcome the much higher propagation loss in the THz-band communication networks. Also, the utilization of ultra-narrow-beam could drastically increase the time needed to conduct a traditional beam search in space [13]–[15]. In many other cases, heuristic approaches are designed to (probabilistically) minimize the neighbor discovery time [16], [17]. Their performance would further be a compromise with narrower beams. Other solutions that rely on tight synchronization through all the nodes in the network [18], [19] may lead to very long discovery time due to the lack of efficient broadcasting capabilities.

In this paper, we present a time-efficient neighbor discovery protocol for directional THz-band communication networks.

We consider that, during the neighbor discovery process, all nodes beam-steer or rotate their DAs in discrete steps, in which transmitters periodically announce their presence and receivers constantly sense the coming signals. If nodes only use the main-lobe information, two nodes can only find each other when their DAs are exactly aligned and facing, which leads to a very long neighbor discovery time. To solve this issue, we suggest to lever-age the full antenna radiation pattern with side-lobes, as opposed to existing protocols, where antenna side-lobes are either ignored or minimized. More specifically, we map the effectively received signals to a universal detection standard, based on which we promptly locate a specific neighbor. In our preliminary works presented in [1], we analytically and numerically showed that, in free space, the neighbor discovery time can be significantly reduced by utilizing our proposed protocol. In this paper, we further test and validate the proposed protocol by utilizing the X60 testbed [20], which is a software-defined-based testbed for broadband wireless communication networks at 60 GHz. In ad-dition, we analyze the feasibility of the proposed protocol in a bounded space, e.g., a square room, where signal reflection is taken into account.

The rest of this paper is organized as follows. In Section II, we describe the topology of the network, the directional antenna model, and the derivation of the received signal power strength. We describe our proposed neighbor discovery protocol in Section III. In Section IV, we mathematically compare the neigh-bor discovery protocols with and without side-lobes information. The analysis is based on free space scenario. We describe the testing process by using X60 testbed and validate the proposed protocol with X60 testing data in Section V. In Section VI, we analyze the feasibility of the proposed protocol inside a bounded square room. In Section VII, we provide numerical results and, finally, we conclude the paper in Section VIII.

II. SYSTEM MODEL

In this section, we describe the system model including the network topology, the antenna model and the received signal power model.

A. Network Topology

The network topology is shown in Fig. 1, where the discov-ering node is marked as RX. The one-hop coverage area A of RX is calculated as:

$$A = \pi R^2, \tag{1}$$

where R is determined by the maximum transmission power of each transmitter.

TX represents a neighboring transmitter that is located within one-hop communication range of RX. All TXs are randomly distributed in A following a spatial Poisson distribution with node density λ_A. Therefore, the total number of TXs within A is given by:

$$N_t = A\lambda_A. \tag{2}$$

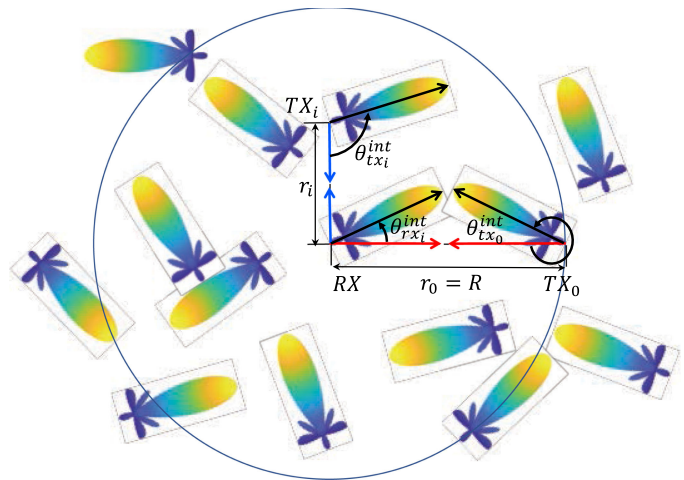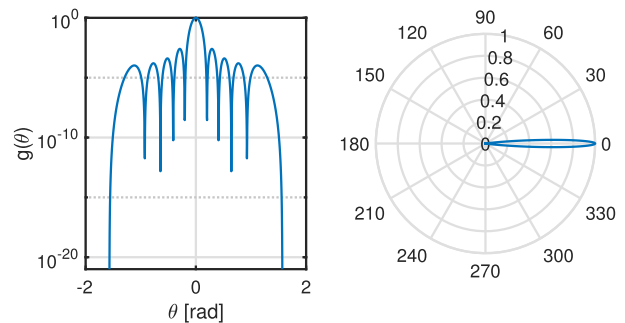Fig. 1. Free space network topology.

Fig. 2. Radiation pattern of 10×10-elements planar array.

B. Antenna Model

We consider all nodes are operating in the same elevation plane. In other words, the antennas' elevation beam angles ϕ are set to zero. In addition, we consider that each node is equipped with a time-delay beamforming antenna array. Hence, the nor-malized power gain pattern of an $N \times N$-elements planar array (with each individual element placed $\lambda/2$ apart) is given by [21]:

$$g(\theta) = \left(\frac{1}{N^2} \frac{\sin^2\left(\frac{N}{2}\pi\sin\theta\right)}{\sin^2\left(\frac{1}{2}\pi\sin\theta\right)} \right)^2, \tag{3}$$

where g stands for the antenna gain including main-lobe and side-lobes. The 2D radiation pattern of a 10×10-elements pla-nar array is shown in Fig. 2 as a reference. In our analysis, we consider that the DAs are rotating and the main features of the radiation pattern are preserved even when beam steering. This is true in the case of mechanical steering, and this is achievable in terms of electrical steering provided the right codebooks are defined.

C. Received Signal Power

The received signal power P_{rx} is constantly changing due to steering of the DAs in both transmission and reception. Con-sequently, P_{rx} denotes the instantaneous power at the receiver

and is a function of time t as well as the initial DA angles of transmitter and receiver, which are denoted as θ_{tx}^{int} and θ_{rx}^{int}, respectively. The turning speeds of the transmitter and the receiver are given by ω_{tx} and ω_{rx}, respectively. These can be either positive or negative, indicating clock-wise or counter-clock-wise directions, respectively. Besides, P_{rx} is also a function of frequency f and distance r between the transmitter and the receiver, given that $r \leq R$. Thus, P_{rx} is formulated as:

$$P_{rx}(r, \theta_{tx}^{int}, \theta_{rx}^{int}, t, f) = \int_{B(r)} S_{tx}(f) G_{\max}^2(f) g(\theta_{tx}^{int} + \omega_{tx}t)$$
$$\times g(\theta_{rx}^{int} + \omega_{rx}t) \frac{c^2}{(4\pi fr)^2} e^{-K_{abs}(f)r} df, \tag{4}$$

where B refers to the 3 dB bandwidth and depends on the transmission distance, S_{tx} represents power spectrum density (p.s.d) of the transmitted signal, $G_{\max}$ is the maximum power pattern of the antennas and K_{abs} stands for the molecular absorption coefficient.

For simplification purposes, we consider the system is operating in a constant 3 dB frequency window with the central frequency f_0. Therefore, the frequency-variant components in (4) are approximated as constant values. In this case, the simplified equation is expressed as:

$$P_{rx}(r, \theta_{tx}^{int}, \theta_{rx}^{int}, t) = \gamma g(\theta_{tx}^{int} + \omega_{tx}t) g(\theta_{rx}^{int} + \omega_{rx}t) r^{-2} e^{-Kr}, \tag{5}$$

where $\gamma = P_{tx} G_{\max}^2(f_0) \frac{c^2}{16\pi^2 f_0^2}$, P_{tx} is the transmitted signal power and $K = K_{abs}(f_0)$ is a constant value.

III. NEIGHBOR DISCOVERY PROTOCOL WITH SIDE-LOBES INFORMATION

In this section, we describe the design logic of the proposed neighbor discovery protocol with side-lobes information.

A. Design Logic of the Proposed Neighbor Discovery Protocol

In lower frequency communication systems, neighbor discovery can be efficiently completed thanks to the possibility to communicate with omni-directional antennas. In fact, the neighbor discovery is achieved as long as the received signal strength P_{rx} is larger than the received Signal to Interference Ratio (SIR) threshold. However, in THz-band communication networks, highly directional communication links are established between transmitters and receivers. The connectivity between node pairs is determined by the transient direction of the DA at each node. Therefore, other than just identifying the neighboring node within one-hop communication range of the detecting node, the neighbor discovery protocol for THz-band communication also needs to detect the corresponding direction of the neighboring node. Nevertheless, it is infeasible to rely only on P_{rx} to obtain the aforementioned information. Seeing that P_{rx}, as described in Section II, is affected by several factors including discovery time t, communication distance r, initial angles

$\theta_{tx}^{int}, \theta_{rx}^{int}$ and turning speeds ω_{tx}, ω_{rx} of the transmitter and receiver, respectively. Thus, without knowing the detailed combination of all the factors, it is infeasible to locate the signal source by just using P_{rx}. For this reason, we present a universal signal pattern, which indicates the potential direction of signal source by mapping enough successively received signal samples to the signal pattern.

To obtain the universal signal pattern, we observe that as long as the distance between the transmitter and the receiver is constant during the neighbor discovery process, during which the transmitter's and the receiver's DAs are turning, the changing rate of the total antenna gain, $\Delta G(t)/\Delta t$, along the directional communication link exhibits a certain signal pattern, where $G(t) = G_{\max}^2 g(\theta_{tx}^{int} + \omega_{tx}t) g(\theta_{rx}^{int} + \omega_{rx}t)$, it stands for the total DAs' gain, $\Delta G(t)$ is derived with a series of continuously received signal samples. Most importantly, the signal pattern is a universal pattern that is irrelevant to the initial angle difference between the transmitter's and the receiver's DAs.

B. Process of Neighbor Discovery With Side-Lobe Information

The process of our proposed neighbor discovery protocol with side-lobes information is illustrated in Fig. 3, where the signal patterns are obtained based on a test case with one transmitter and one receiver, each utilizing a 10×10-elements planar array. In the scenario under analysis, the transmitter's DA and the receiver's DA turn at constant speeds with different directions ($\omega_{tx} = -\omega_{rx}$). From the receiver's perspective, $\Delta G(t)/\Delta t$ signal pattern is symmetrical in respect to the axis that points from the receiver to the transmitter. With the main-lobe of the receiver's DA steering further away from the direction of the transmitter, the changing rate of the received signal samples gradually weaken. Thus, we analyze the received signal pattern within a certain angle range, namely, from 0 to $\pi/2$ in respect to the axis that points from the receiver to the transmitter. In our analysis, we monitor instead the changes in the equivalent electric-field intensity of the antenna $\Delta E(t)/\Delta t$ with $E(t) = 10^{\frac{G(t)}{20}}$ to observe more distinguished features.

In the upper plot of Fig. 3(a), as the main-lobe of the receiver's DA rotates away from the direction that points towards the transmitter, the signal pattern of $\Delta E(t)/\Delta t$ fluctuates over the passed angle and progressively becomes weak. Any new $\Delta E(t)/\Delta t$ data sample on the y-axis can be mapped to n potential directions on the x-axis, with $n \geq 2$. Thus, based on the mapping property between the received data samples and the potential direction of the neighbor, the $\Delta E(t)/\Delta t$ sample pattern is classified into two categories. On the one hand, data samples in the green-shaded region can be uniquely mapped to a specific direction one-to-one. Thanks to the opposite trends of data samples' changing rate, i.e., increase and decrease, only two continuous $\Delta E(t)/\Delta t$ data samples are needed to complete the unique mapping. On the other hand, the pink-shaded region exhibits a one-to-n mapping property. In this case, it is difficult to achieve neighbor discovery by only using $\Delta E(t)/\Delta t$ signal pattern. An additional $d^2E(t)/dt^2$ signal pattern is needed, which is calculated based on the same scenario by taking the second derivative

(a) Signal pattern of $dE(t)/dt$ (b) Signal pattern of $d^2E(t)/dt^2$ (c) Signal pattern of $d^3E(t)/dt^3$
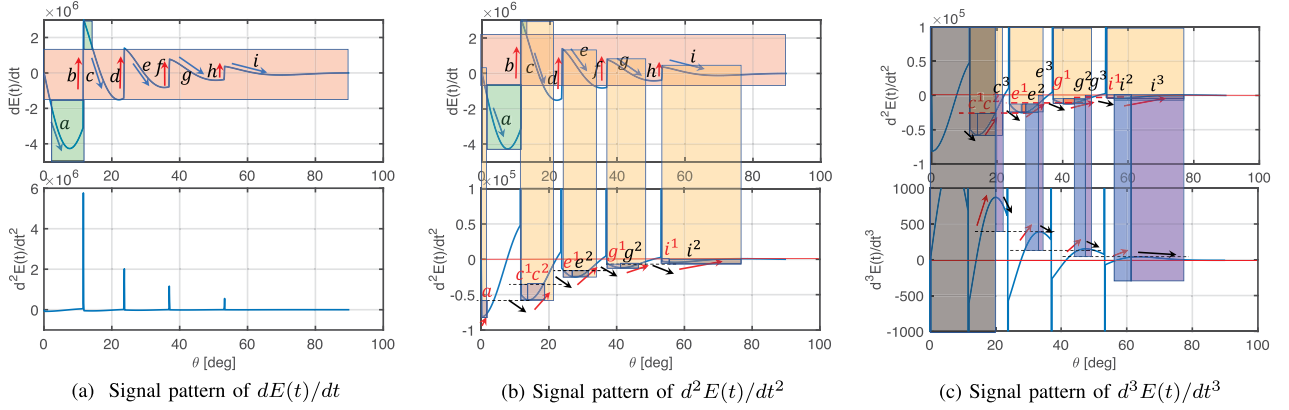
Fig. 3. Impact of side-lobe information in neighbor discovery.

of $E(t)$, and shown as the bottom plot of Fig. 3(a). In $d^2E(t)/dt^2$ signal pattern, the positive sharp pulses indicate the drastically increasing parts in $\Delta E(t)/\Delta t$ signal pattern. Consequently, different amplitudes of the positive pulses in $d^2E(t)/dt^2$ signal pattern correspondingly indicate the potential neighboring directions of b, d, f and h parts in $\Delta E(t)/\Delta t$ signal pattern.

The zoomed-in plot of the negative parts of $d^2E(t)/dt^2$ signal pattern is illustrated in the bottom plot of Fig. 3(b). The correlated parts between the negative parts of $d^2E(t)/dt^2$ signal pattern and the decreasing parts of $\Delta E(t)/\Delta t$ signal patterns are marked by yellow-shaded boxes. We observe that $d^2E(t)/dt^2$ signal pattern can also be classified as two categories based on the data samples' mapping property. In particular, the one-to-one mapping property is shown in the fractions of a, c^1, c^2, e^1, g^1 and i^1 in $d^2E(t)/dt^2$ signal pattern. Thus, the received $d^2E(t)/dt^2$ data samples which are mapped into these regions can be directly leveraged in neighbor discovery. Otherwise, due to the one-to-n mapping property, a higher order derivative signal pattern is needed as an assistance.

As presented in Fig. 3(c), an additional $d^3E(t)/dt^3$ signal pattern is utilized. So far, those undetermined parts in $d^2E(t)/dt^2$ signal pattern can be further detected by utilizing $d^3E(t)/dt^3$ signal pattern. In particular, most undetermined fractions in $d^2E(t)/dt^2$ signal pattern exhibit one-to-one mapping property in $d^3E(t)/dt^3$ signal pattern, in light of either increasing changing rate, e.g., e^2, g^2 and i^2, or decreasing changing rate, e.g., c^3, e^3, g^3 and i^3. As a consequence, the most potential directions can be effectively detected with the cooperation of the aforementioned signal patterns. For remaining uncertain directions, we can either apply a higher order derivative signal pattern as an assistance or map the rest of uncertain potential directions in $d^2E(t)/dt^2$ signal pattern, which have distinct differences as shown with the very small red-shaded blocks in the upper plot of Fig. 3(c). The selection changes for different scenarios, depending on the weight of the uncertain parts.

IV. PROTOCOL COMPARISON

In this section, we mathematically analyze and compare the performance in free space of two different neighbor discovery protocols, namely, without and with side-lobes information.

The latter is based on the proposed protocol we described in Section III. We first analyze the delay associated to the discovery of a single node, and then extend our analysis to the discovery of all one-hop neighbors of the receiver.

A. Neighbor Discovery Without Side-Lobes Information

For the neighbor discovery protocol without side-lobes information, the sufficient condition of an effective neighbor discovery is to completely align the main-lobes of the transmitter's and the receiver's DAs and adjust their main-lobes to face toward each other. This prerequisite guarantees that the signal strength received by the main-lobe of RX is strong enough to detect any TX located within A. We represent the discovery process as a random process $X(\theta_{tx}^{int}, \theta_{rx}^{int}, t)$ formulated as:

$$X(\theta_{tx}^{int}, \theta_{rx}^{int}, t) = g(\theta_{tx}^{int} + \omega_{tx}t)g(\theta_{rx}^{int} + \omega_{rx}t), \quad (6)$$

where θ_{tx}^{int} and θ_{rx}^{int} stand for the initial angles of the transmitter's DA and the receiver's DA, respectively. As shown in Fig. 1, these angles are defined in respect to the direction of alignment between the transmitter and the receiver. ω_{tx} and ω_{rx} are the turning speeds of the transmitter and the receiver as described in Section II.

When the condition $X(\theta_{tx}^{int}, \theta_{rx}^{int}, t) = 1$ is satisfied, the RX discovers a specific node TX_0. The variables $\theta_{tx}^{int}, \theta_{rx}^{int}$ are uniformly distributed from $-\pi$ to π and, thus, their p.d.f is $1/2\pi$. The variable t is uniformly distributed in time duration $[0, T]$ and its p.d.f is $1/T$. The probability for RX to discover TX_0 is therefore given by:

$$P_{find}^{one} = \int_{t=0}^{T} \int_{\theta_{rx}^{int}=-\pi}^{\pi} \int_{\theta_{tx}^{int}=-\pi}^{\pi} \mathbf{1}\left(X(\theta_{tx}^{int}, \theta_{rx}^{int}, t) == 1\right)$$

$$\times \frac{1}{4\pi^2} \frac{1}{T} d\theta_{rx}^{int} d\theta_{tx}^{int} dt = \frac{E\left[T_{find}^{one}\right]}{T}, \quad (7)$$

where $\mathbf{1}(\cdot)$ is an indicator function that equals 1 when the argument is true and 0 otherwise. $E[T_{find}^{one}]$ refers to the expected time for RX to discover a specific TX_0, which is calculated by
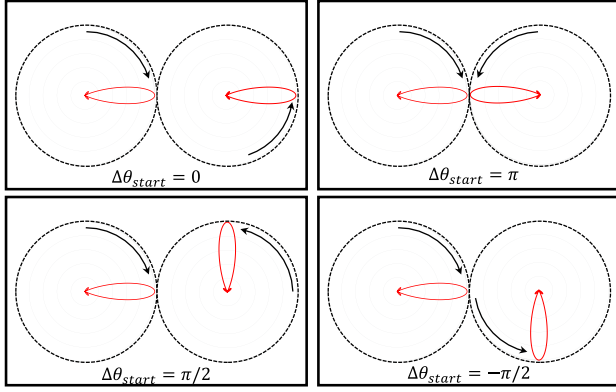
Fig. 4.   Facing probability.

multiplying T on both sides of (7). Thus,

$$
E\left[T_{find}^{one}\right] = \int_{t=0}^{T}\int_{\theta_{rx}^{int}=-\pi}^{\pi}\int_{\theta_{tx}^{int}=-\pi}^{\pi}\mathbf{1}\left(X(\theta_{tx}^{int},\theta_{rx}^{int},t)==1\right)
$$
$$
\times\,\frac{1}{4\pi^2}d\theta_{rx}^{int}d\theta_{tx}^{int}dt. \tag{8}
$$

In order to find all TXs within one-hop communication range of the RX, we consider the neighbor discovery process of each node is independent, and RX cannot discover several TXs simultaneously. Thus, the expected time to discover all TXs is calculated as:

$$
E\left[T_{find}^{all}\right] = \sum_{i=1}^{N_t}P_{find}^{one}E\left[T_{find}^{one}\right] = N_t P_{find}^{one}E\left[T_{find}^{one}\right]. \tag{9}
$$

We would like to emphasize that $E[T_{find}^{one}]$ may go to infinite. Because in the neighbor discovery scheme with only main-lobe information, transmitter and receiver may never meet each other. This happens when the initial angle difference of the transmitter's DA and the receiver's DA is not π as shown in Fig. 4. However, this is not a problem in our proposed protocol as we explain next.

B. Neighbor Discovery With Side-Lobes Information

Based on the description in Section III, we know that as long as RX successfully receives enough continuous signal samples from a specific neighbor TX_0, it will be able to map the received signal samples to the universal signal pattern and to locate the specific neighbor. The issue in this scenario is that RX may not be able to detect TX_0 immediately, even if they are located close to each other. This problem occurs when the DAs' main-lobes deviate from the direction that aligns them and, thus, the instantaneous SIR detected by RX is insufficient to surpass the SIR threshold β. However, our proposed protocol only considers the continuous signals whose power strength surpasses β as effective signals to accomplish the neighbor discovery process.

Assuming TX_0 is locate r_0 away from RX. The received signal power at the RX is calculated as:

$$
P_{rx}^{0}(r_0,\theta_{tx_0}^{int},\theta_{rx_0}^{int},t)
$$
$$
= \gamma g(\theta_{tx_0}^{int}+\omega_{tx}t)g(\theta_{rx_0}^{int}+\omega_{rx}t)r_0^{-2}e^{-Kr_0}, \tag{10}
$$

where $\theta_{tx_0}^{int}$ and $\theta_{rx_0}^{int}$ represent initial angles of the transmitter's DA and the receiver's DA, respectively.

The interference occurs when another neighbor TX_i transmits signals to RX simultaneously with TX_0. The interference caused by TX_i is calculated as:

$$
I(r_i,\theta_{tx_i}^{int},\theta_{rx_i}^{int},t)
$$
$$
= \gamma g(\theta_{tx_i}^{int}+\omega_{tx}t)g(\theta_{rx_i}^{int}+\omega_{rx}t)r_i^{-2}e^{-Kr_i}, \tag{11}
$$

where r_i is the distance between TX_i and RX.

We consider TX_i is uniformly distributed within the one-hop coverage area of RX. Thus, the c.d.f of r_i is calculated as:

$$
F_X(r_i) = \frac{\pi r_i^2}{\pi R^2} = \frac{r_i^2}{R^2}. \tag{12}
$$

Hence, the p.d.f of r_i is $\frac{2r_i}{R^2}$. Considering each node is independent with others, the expected value of interference caused by all the interfering neighbors is given by:

$$
E(I) = (N_t-1)\int_{t=0}^{T}\int_{\theta_{tx_i}^{int}=-\pi}^{\pi}\int_{\theta_{rx_i}^{int}=-\pi}^{\pi}\int_{r_i=0}^{R}
$$
$$
I(r_i,\theta_{tx_i}^{int},\theta_{rx_i}^{int},t)\frac{2r_i}{R^2}\frac{1}{4\pi^2}\frac{1}{T}dr_i d\theta_{rx_i}^{int}d\theta_{tx_i}^{int}dt. \tag{13}
$$

For any pair of communicating nodes, the SIR is calculated as:

$$
S(r_0,\theta_{tx_0}^{int},\theta_{rx_0}^{int},t) = P_{rx}^{0}(r_0,\theta_{tx_0}^{int},\theta_{rx_0}^{int},t)E\left[\frac{1}{I}\right], \tag{14}
$$

where $E[\frac{1}{I}]$ is given by [22]:

$$
E\left[\frac{1}{I}\right] = f(\mu_0)+\frac{f''(\mu_0)}{2}\sigma^2[I], \tag{15}
$$

where $\mu_0 = E[I]$, which is the mean value of the random variable I. We define $f(\mu_0) = \frac{1}{\mu_0} = \frac{1}{E[I]}$, thus, $f''(\mu_0) = \frac{2}{\mu_0^3} = \frac{2}{(E[I])^3}$. $\sigma^2[I]$ is the variance of random variable I and is calculated as $\sigma^2[I] = E[I^2]-(E[I])^2$. After simplification, (15) can be rewriten as:

$$
E\left[\frac{1}{I}\right] = \frac{E\left[I^2\right]}{E[I]^3}, \tag{16}
$$

where $E[I^2]$ is expressed as:

$$
E[I^2] = (N_t-1)\int_{t=0}^{T}\int_{\theta_{rx_i}^{int}=-\pi}^{\pi}\int_{\theta_{tx_i}^{int}=-\pi}^{\pi}\int_{r_i=0}^{R}
$$
$$
\times I^2(r_i,\theta_{tx_i}^{int},\theta_{rx_i}^{int},t)\frac{2r_i}{R^2}\frac{1}{4\pi^2}\frac{1}{T}dr_i d\theta_{rx_i}^{int}d\theta_{tx_i}^{int}dt. \tag{17}
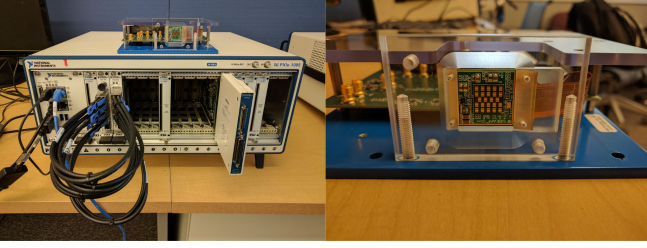$$

Fig. 5.   The X60 testbed.

The interference at RX is created by all surrounding TX_i. Thus, the probability that RX discovers a specific TX_0 by receiving an effective signal sample is given by:

$$P_{find}^{one} = \int_{t=0}^{T} \int_{\theta_{rx_0}^{int}=-\pi}^{\pi} \int_{\theta_{tx_0}^{int}=-\pi}^{\pi} \int_{r_0=0}^{R}$$
$$\times \mathbf{1}\left(S(r_0, \theta_{tx_0}^{int}, \theta_{rx_0}^{int}, t) \geq \beta\right) \frac{2r_0}{R^2} \frac{1}{4\pi^2} \frac{1}{T} dr_0 d\theta_{rx_0}^{int} d\theta_{tx_0}^{int} dt. \tag{18}$$

Thus, the total time to discover all neighbors of RX is calculated as:

$$E[T_{find}^{all}] = \sum_{i=1}^{N_t} P_{find}^{one}(N_s\Delta t) = N_t P_{find}^{one}(N_s\Delta t), \tag{19}$$

where N_t refers to the total number of one-hop neighbors of RX derived in (2). N_s is the number of the continuously received effective data samples that are utilized to achieve the neighbor discovery process. For example, in the scenario of utilizing up to the third order derivative of the signal pattern, $N_s = 5$, which is calculated by converting the number of received data samples from the highest order derivative of $E(t)$ down to $E(t)$. $1/\Delta t$ is the received signal sample rate. In this paper, we test with the slowest sample rate by considering the antenna rotates sector by sector, thus:

$$\Delta t = \frac{\min\left(\theta_{bw}^{tx}, \theta_{bw}^{rx}\right)}{|\omega_{rx} - \omega_{tx}|}, \tag{20}$$

where θ_{bw}^{tx} and θ_{bw}^{rx} are sector beamwidths of the transmitter's DA and the receiver's DA, rerspectively.

In the preliminary version of this work [1], we conducted numerical results evaluating the comparison of two different neighbor discovery protocols, i.e., without and with side-lobes information. In next section, we test our protocol with data samples collected with the X60 testbed.

V. X60 TESTING

In this section, we test our proposed neighbor discovery protocol with the X60 testbed (Fig. 5), a software-defined-based testbed for broadband wireless communication networks at 60 GHz [23].

The X60 system provides a high level of reconfigurability across the physical, link and network layers. Its bandwidths and speeds commensurate to the IEEE 802.11ad standard. The mmWave transceiver covers the 60 GHz frequency band for channel sounding and real-time communication with coding. In this test, we configure a SISO uni-directional communication
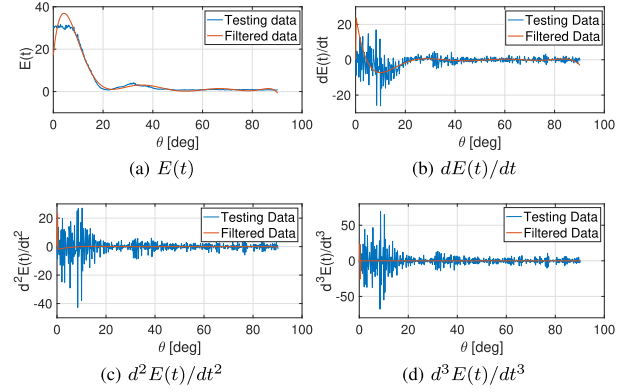

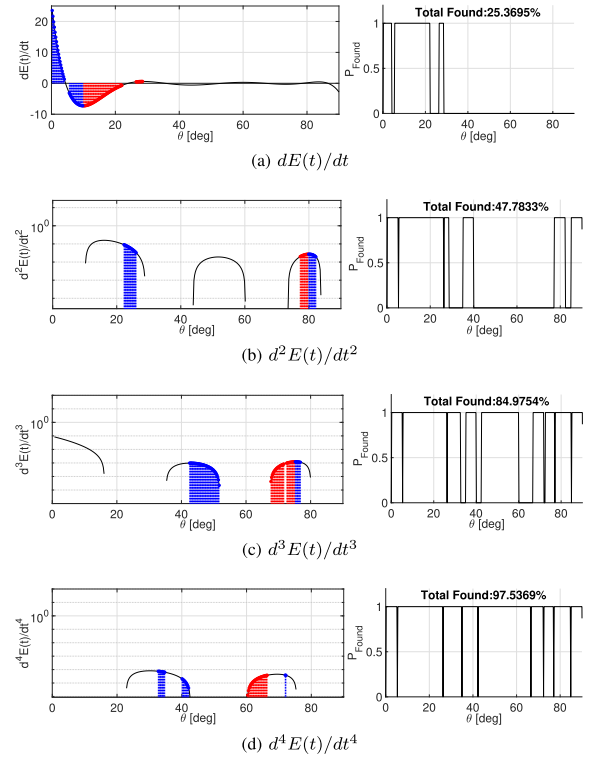Fig. 6.   Processing of the testing data.

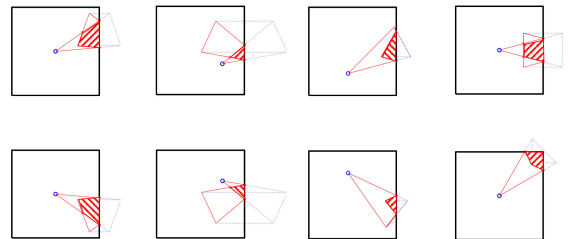Fig. 7.   Neighbor discovery protocol with side-lobe information.

Fig. 8.   Reflection patterns of the beam in the room.

link with both transmitter and receiver applying the same settings of DA beam pattern. To obtain the universal signal pattern, we set the transmitter DA and the receiver DA to continuously sweep the entire area with a constant turning speed, however, in different directions.

The collected raw testing data is shown as the blue curve in Fig. 6a, which is corrupted by noise. As shown in the rest of

(a) O $(0,0)$ (b) O $(0,3.5)$ (c) O $(0,7)$ (d) O $(0,9.9)$ (e) O $(0,-3.5)$ (f) O $(0,-7)$ (g) O $(0,-9.9)$

(h) O $(-2.5,-9)$ (i) O $(-2.5,-7)$ (j) O $(-2.5,-5)$ (k) O $(1.5,1.5)$ (l) O $(3.5,3.5)$ (m) O $(7,7)$ (n) O $(9.9,9.9)$
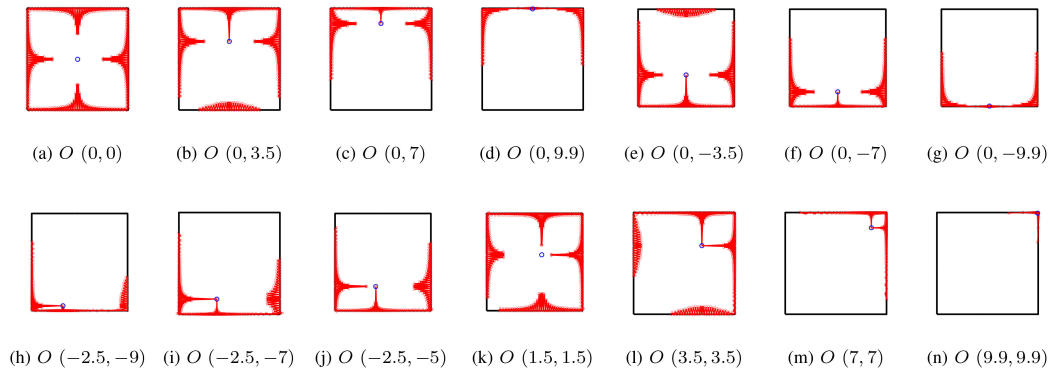
Fig. 9.   Impact area in the room.

the sub-figures in Fig. 6, the fluctuations of the higher order derivative signal patterns increase and can not be directly used as the universal signal patterns. In this case, we first filter the raw testing data with a low pass filter. The filtered signal pattern is shown as the red curve in Fig. 6a. Then, we utilize the higher order derivatives of the filtered data as the universal detection standard for neighbor discovery.

Further, we apply the proposed neighbor discovery protocol with side-lobes information to X60 testing. Based on the signal pattern of $dE(t)/dt$ shown in Fig. 7a, the detection results of the uniquely decreasing or increasing $dE(t)/dt$ data samples are marked as the blue or red dots, respectively, which locate approximate 25.37% of the neighbor directions. With a higher order derivative of the signal pattern, the detection process only needs to be applied in the remaining possible directions. We observe that approximate 97.54% of potential directions are found with up to the fourth order derivative of the received signal samples, which means only 6 consecutively received signal samples are enough to locate the neighboring node. This result validates our previous hypothesis.

VI. NEIGHBOR DISCOVERY IN A SQUARE ROOM WITH REFLECTION

In this section, we analyze the feasibility of the proposed neighbor discovery protocol in a bounded space, e.g., a square room, where the transmitted signal power can be reflected by the walls. In this case, an impact area A_I is formed in the overlapped area of the reflected signal and the transmitted signal, where the aforementioned signal pattern will be destroyed. To estimate the expected size of the impact area, we use an idealized antenna model in our analysis. The antenna beam only consists of the main lobe with a cone-shaped power pattern. In Fig. 8, we summarize all possible reflected patterns of an idealized antenna beam inside a room, where the impact area is marked by the shaded area.

When rotating the DA, the total impact area for the node is formed by accumulating the impact area at each steering sector. In Fig. 9, the total impact area generated by a node with the DA beamwidth $\theta_{bw} = 2^o$ and the transmission distance d as half of the length of the wall is shown. We observe that the total impact area highly depends on the location of the node and its position relative to the walls.

To derive the expected size of the impact area for a node, we assume the node is located in a square room with the length of each wall equals $2l$, as shown in Fig. 10. The position of the node is marked as (x,y) in the coordinate system. The coordinates of the corners of the room are $(l,l), (-l,l), (-l,-l)$ and $(l,-l)$, separately. The extensions of the boundary lines of the node's DA beam are denoted as l'_1 and l'_2. They start at (x,y) and are terminated by the walls. The orientation of the DA beam is defined as the angle between the counterclockwise rotating l'_1 and the positive direction of x-axis. The beamwidth θ_{bw} of the DA is a function of the transmission distance d of the node, which is calculated as [24]:

$$\theta_{bw}(d) \leq \sqrt{4\pi \sqrt{\frac{\int_{B(d)} S_{tx}(f)\frac{c^2}{(4\pi df)^2} e^{-K_{abs(f)} d} df}{N_r(d) SNR_{min}}}}, \quad (21)$$

where N_r is the molecular absorption noise power, SNR_{min} stands for the minimum SNR threshold.

Considering the different geometrical relationship of the polygon of the impact area per sector, the room can be classified into 4 categories, which depend on the length of l'_1 and l'_2, which represent the distance from the node to the wall along the two edges of cone shape power pattern, respectively. As shown in Fig. 10, we observe that $l'_1 < l'_2$ is always true in the union set of $\{A_1, A_3, A_5, A_7\}$, and the union set of $\{A_2, A_4, A_6, A_8\}$ is formed by meeting the condition of $l'_1 > l'_2$. In the union set of $\{Z_1, Z_3, Z_5, Z_7\}$, we observe that $l'_1 = l'_2$, and l'_1 approximately equals to l'_2 in the union set of $\{Z_2, Z_4, Z_6, Z_8\}$.

In order to decrease the calculation complexity caused by polygons with different number of edges as shown in Fig. 8, we assume the impact area per sector is always a triangle. Under this assumption, we can further simplify the classification of the room area by composing new area A'_i with Z_i and A_i, for any integer $i \in [1,8]$. Thus, the room area can be represented by only two categories. For the class of $l'_1 \leq l_2'$, the area sets include $\{A'_1, A'_3, A'_5, A'_7\}$, and for the class of $l_1' \geq l'_2$, the area sets include $\{A'_2, A'_4, A'_6, A'_8\}$. To calculate the area of each impact triangle, the base and the height of the triangle are denoted as l_3 and h, respectively, where l_3 is the line section that the DA beam intersects with the reflecting wall, and h is the maximum vertical distance between the reflected signal and the reflecting wall. We use l_1 and l_2 to represent the line sections of the edges of the DA's beam before been reflected, l_1 and l_2 are part of l'_1
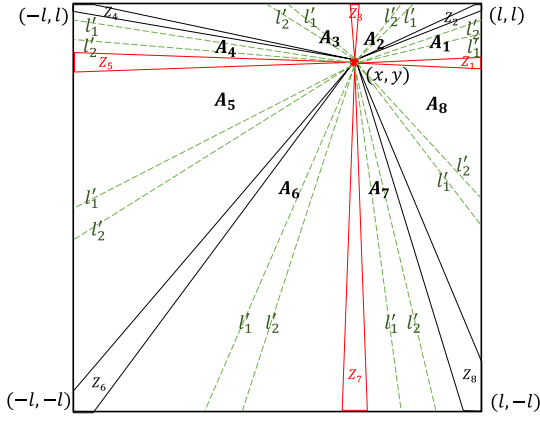
Fig. 10. Reflection inside a room.

and l_2', respectively. The expect impact area in each area sets can be separately calculated as:

$$E[A_i'] = \frac{1}{2l}\frac{1}{2l}\frac{1}{2\pi}\int_{-l}^{l}\int_{-l}^{l}\int_{\theta \in \theta_{A_i'}} \frac{l_3^{A_i'} h^{A_i'}}{2} d\theta dx dy. \tag{22}$$

The detailed derivation of the geometrical functions of each component in (22) is provided in the Appendix.

Thus, the total expected impact area for a node inside the square room can be calculated as (23) shown at the bottom of this page, where $F_{\sin}$ and $F_{\cos}$ can be expressed as:

$$F_{\sin}(d) = \frac{1}{2}\sqrt{\frac{1}{(\sin(x))^2} + \frac{1}{(\sin(\theta + \theta_{bw}(d)))^2} - 2\left(\frac{\cos(\theta_{bw}(d))}{\sin(\theta)\sin(\theta + \theta_{bw}(d))}\right)},$$

$$F_{\cos}(d) = \frac{1}{2}\sqrt{\frac{1}{(\cos(x))^2} + \frac{1}{(\cos(\theta + \theta_{bw}(d)))^2} - 2\left(\frac{\cos(\theta_{bw}(d))}{\cos(\theta)\cos(\theta + \theta_{bw}(d))}\right)}. \tag{24}$$

Because the proposed neighbor discovery protocol can only work in the non-impact area where the signal pattern is not destroyed by the reflection, we combine both the proposed protocol and the protocol without side-lobe information for neighbor discovery in a bounded space. The discovering node should switch to use the protocol without side-lobe information when the received signal does not follow the universal data pattern. The expected time for a node to discover its neighbor inside a square room is calculated as:

$$E\left[T_{find}^{SIR_{\max}+SIR_\beta}\right] = T_{find}^{SIR_\beta}\overline{P_I}^2 + T_{find}^{SIR_{\max}}\left(1 - \overline{P_I}^2\right), \tag{25}$$

$$E[A_I(d)] = E[A_I^1(d)] + E[A_I^2(d)] + E[A_I^3(d)] + E[A_I^4(d)] + E[A_I^5(d)] + E[A_I^6(d)] + E[A_I^7(d)] + E[A_I^8(d)]$$

$$= \frac{1}{2l}\frac{1}{2l}\frac{1}{2\pi}\int_{-l}^{l}\int_{-l}^{l}\left(\int_{-\frac{\theta_{bw}(d)}{2}}^{\arctan\left(\frac{l-y}{l-x}\right)-\frac{\theta_{bw}(d)}{2}}(l-x)F_{\cos}(d)\left(d - \frac{l-x}{\cos(\theta)}\right)\cos(\theta)d\theta\right.$$

$$+ \int_{\arctan\left(\frac{l-y}{l-x}\right)-\frac{\theta_{bw}(d)}{2}}^{\frac{\pi}{2}-\frac{\theta_{bw}(d)}{2}}(l-y)F_{\sin}(d)\left(d - \frac{l-y}{\sin(\theta + \theta_{bw}(d))}\right)\sin(\theta)d\theta$$

$$+ \int_{\frac{\pi}{2}-\frac{\theta_{bw}(d)}{2}}^{\pi+\arctan\left(\frac{l-y}{-l-x}\right)-\frac{\theta_{bw}(d)}{2}}(l-y)F_{\sin}(d)\left(d - \frac{l-y}{\sin(\theta)}\right)\sin(\theta)d\theta$$

$$+ \int_{\pi+\arctan\left(\frac{l-y}{-l-x}\right)-\frac{\theta_{bw}(d)}{2}}^{\pi-\frac{\theta_{bw}(d)}{2}}(l+x)F_{\cos}(d)\left(d + \frac{l+x}{\cos(\theta + \theta_{bw}(d))}\right)(-\cos(\theta))d\theta$$

$$+ \int_{\pi-\frac{\theta_{bw}(d)}{2}}^{\pi+\arctan\left(\frac{-l-y}{-l-x}\right)-\frac{\theta_{bw}(d)}{2}}(l+x)F_{\cos}(d)\left(d + \frac{l+x}{\cos(\theta)}\right)(-\cos(\theta))d\theta$$

$$+ \int_{\pi+\arctan\left(\frac{-l-y}{-l-x}\right)-\frac{\theta_{bw}(d)}{2}}^{\frac{3\pi}{2}-\frac{\theta_{bw}(d)}{2}}(l+y)F_{\sin}(d)\left(d + \frac{l+y}{\sin(\theta + \theta_{bw}(d))}\right)(-\sin(\theta))d\theta$$

$$+ \int_{\frac{3\pi}{2}-\frac{\theta_{bw}(d)}{2}}^{\arctan\left(\frac{-l-y}{l-x}\right)-\frac{\theta_{bw}(d)}{2}}(l+y)F_{\sin}(d)\left(d + \frac{l+y}{\sin(\theta)}\right)(-\sin(\theta))d\theta$$

$$+ \left.\int_{\arctan\left(\frac{-l-y}{l-x}\right)-\frac{\theta_{bw}(d)}{2}}^{2\pi-\frac{\theta_{bw}(d)}{2}}(l-x)F_{\cos}(d)\left(d - \frac{l-x}{\cos(\theta + \theta_{bw}(d))}\right)\cos(\theta)d\theta\right) dx dy. \tag{23}$$

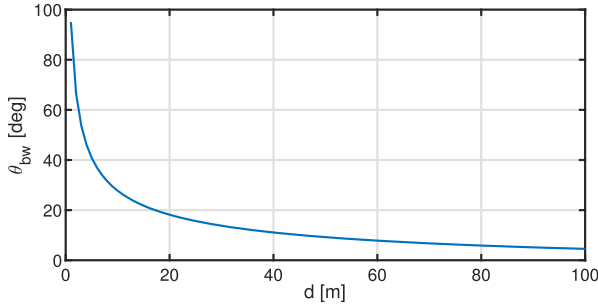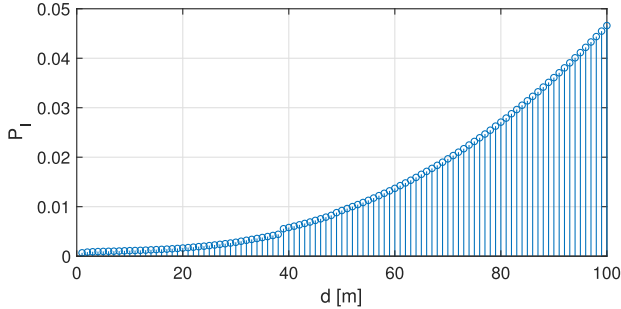Fig. 11.   Beamwidth of ideal directional antenna.

Fig. 13.   Neighbor discovery in free space.

Fig. 12.   Percentage of the impact area in the square room.

Fig. 14.   Neighbor discovery in the square space.

where $T_{find}^{SIR_\beta}$ and $T_{find}^{SIR_{\max}}$ stand for the time duration of discovering a specific neighbor in free space by using the neighbor discovery protocol with and without the side-lobe information, respectively. $\overline{P_I} = 1 - P_I$, and $P_I = \frac{E[A_I]}{A}$ is the probability that a node locates in the impact area, A stands for the total area of the room. The proposed neighbor discovery protocol only works when both transmitter and receiver are located in the non-impact area.

VII. NUMERICAL RESULTS

In this section, we numerically test the performance of our proposed solution for the wall-bounded scenario described above. More specifically, the maximum transmission distance $d_{\max}$ of a node is 100 m, the length of the diagonal line of the bounded space is $2d_{\max}$. The transmission power P_{tx} is -20 dBm, the SIR threshold β is 10 dB, the maximum power pattern $G_{\max}$ of the antennas is 40 dB, the central frequency f_0 is 1.03 THz (i.e., the first absorption-defined window above 1 THz), the transmitter's and receiver's DAs turn in the same speed but with opposite directions. We consider a constant background noise of -110 dBm. The performance of the neighbor discovery protocol with side-lobes information in free space has been analyzed in Section V.

In Fig. 11, we plot the beamwidth variation of the idealized antenna model in respect to the increase of the transmission distance based on (21). Nodes need to narrower the DA's beamwidth to establish longer communication distance.

Fig. 12 shows the percentage of the impact area for one node in the square room. When the transmission distance is very short, the transmitted signal hardly reaches any wall unless the transmitter is very close to the wall. In any case, the size of the impact
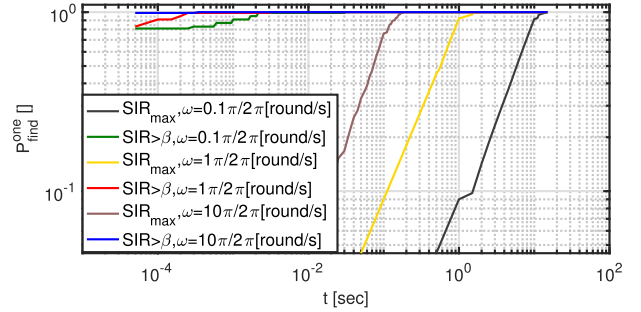
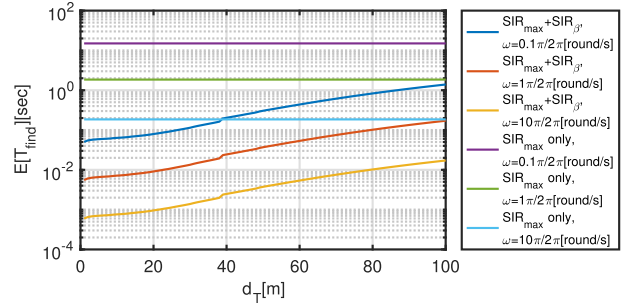area is very small due to the limited transmission distance. With the increasing of the transmission distance, there is higher probability for the antenna beam to reach the walls and, thus, the percentage of the impact area grows.

In Fig. 13, we test the performance of finding a specific neighbor in free space with different neighbor discovery protocols as we described in Section IV, i.e., with and without side-lobes, indicated as SIR_β and $SIR_{\max}$, respectively. The neighbor discovery protocol without side-lobes information requires complete alignment and facing of the transmitter's main-lobe and receiver's main-lobe. The probability of discovering a specific neighbor, as described in (7), increases slowly with time. Before the discovering node completely finds the specific neighbor, i.e., when P_{find}^{one} approach to 1, it already consumed more time than that of the proposed protocol. As a comparison, our proposed neighbor discovery protocol takes the advantage of utilizing side-lobes. As described in (18), whenever the received SIR surpasses the β, the effective signal is successfully received and assisted in neighbor detection. The discovering node find the specific neighbor much faster than the protocol without side-lobes information. We also observe that, faster DAs' turning speeds accelerate the neighbor discovery process and, thus, cause P_{find}^{one} to approach to 1 faster.

In Fig. 14, we test the performance of finding a specific neighbor in a square room, as described in Section VI, with different neighbor discovery protocols. Since the signal pattern can be destroyed by the reflection, the proposed neighbor discovery protocol with side-lobes information cannot work appropriately in the impact area. Thus, we combine two neighbor discovery protocols as described in (25) and denote it as $SIR_{\max} + SIR_\beta$. More specifically, the neighbor discovery protocol without side-lobes is applied in the impact area and the proposed neighbor

discovery protocol is used in the non-impact area. The result shows that, comparing with the neighbor discovery protocol without side-lobes, the combined neighbor discovery protocol greatly reduces the neighbor discovery duration. Besides, due to the fact that more impact area will be formed by increasing the transmission distance of the nodes, the weight of applying the proposed protocol decreases and, thus, more neighbor discovery time is needed. The values of $T_{find}^{SIR_{max}}$ and $T_{find}^{SIR_\beta}$ that we used to derive this results is based on the results from neighbor discovery in free space, as shown in Fig. 13.

VIII. CONCLUSION

In this paper, we have proposed an expedited neighbor discovery protocol that leverages antenna side-lobes information. The direction mapping scheme for the received signal samples has been devised and analyzed. A comparison between our proposed protocol and the protocol without side-lobes has been mathematically analyzed and derived. The proposed protocol has further been tested and validated by utilizing the X60 testbed. An analysis of the feasibility of the proposed protocol in a bounded square room has been conducted as well. The numerical results have been provided to illustrate the improvement of our proposed neighbor discovery protocol in both free space and bounded square space where reflection is taken into account. As a part of the future work, we will understand how multi-path propagation coming not only from walls but from obstacles may affect the proposed protocol, and we will quantify this impact.

APPENDIX

In this section, we derive the geometrical functions of each component in (22), which is utilized in Section VI. For the union set of $\{A_1', A_3', A_5', A_7'\}$ and the union set of $\{A_2', A_4', A_6', A_8'\}$, the angle range of each area from the perspective of the discovering node, is calculated as:

$$\theta_{A_1'} \in \left(-\frac{\theta_{bw}(d)}{2}, arctan\left(\frac{l-y}{l-x}\right) - \frac{\theta_{bw}(d)}{2} \right)$$

$$\theta_{A_3'} \in \left(\frac{\pi}{2} - \frac{\theta_{bw}(d)}{2}, \pi + arctan\left(\frac{l-y}{-l-x}\right) - \frac{\theta_{bw}(d)}{2} \right)$$

$$\theta_{A_5'} \in \left(\pi - \frac{\theta_{bw}(d)}{2}, \pi + arctan\left(\frac{-l-y}{-l-x}\right) - \frac{\theta_{bw}(d)}{2} \right)$$

$$\theta_{A_3'} \in \left(\frac{3\pi}{2} - \frac{\theta_{bw}(d)}{2}, \pi + arctan\left(\frac{-l-y}{l-x}\right) - \frac{\theta_{bw}(d)}{2} \right)$$

$$\theta_{A_2'} \in \left(arctan\left(\frac{l-y}{l-x}\right) - \frac{\theta_{bw}(d)}{2}, \frac{\pi}{2} - \frac{\theta_{bw}(d)}{2} \right)$$

$$\theta_{A_4'} \in \left(\pi + arctan\left(\frac{l-y}{-l-x}\right) - \frac{\theta_{bw}(d)}{2}, \pi - \frac{\theta_{bw}(d)}{2} \right)$$

$$\theta_{A_6'} \in \left(\pi + arctan\left(\frac{-l-y}{-l-x}\right) - \frac{\theta_{bw}(d)}{2}, \frac{3\pi}{2} - \frac{\theta_{bw}(d)}{2} \right)$$

$$\theta_{A_8'} \in \left(\pi + arctan\left(\frac{-l-y}{l-x}\right) - \frac{\theta_{bw}(d)}{2}, 2\pi - \frac{\theta_{bw}(d)}{2} \right)$$
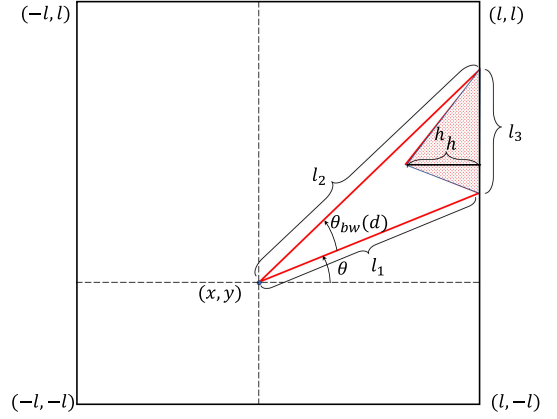

Fig. 15. Impact triangle of the union set of A_1'.

Besides, based on the geometrical relationship of the triangle, the base and the height of the impact triangle are calculated based on the information of l_1 and l_2. For example, based on the union set A_1' shown in Fig. 15, we have:

$$\begin{cases} \dfrac{l-x}{l_1} = \cos(\theta), \\ \dfrac{l-x}{l_2} = \cos(\theta + \theta_{bw}(d)). \end{cases} \quad (26)$$

We can further derive the base l_3 and the hight h of the impact triangle of A_1':

$$A_1' \begin{cases} l_1 = \dfrac{l-x}{cos(\theta)}, \quad l_2 = \dfrac{l-x}{\cos(\theta + \theta_{bw}(d))} \\ l_3 = \sqrt{l_1^2 + l_2^2 - 2l_1 l_2 \cos(\theta_{bw}(d))} \\ h = (d - l_1)\cos(\theta) \end{cases}$$

Then, we derive the geometrical relationship of the impact triangle for the rest union sets based on the same methodology and we have:

$$A_3' \begin{cases} l_1 = \dfrac{l-y}{\sin(\theta)}, \quad l_2 = \dfrac{l-y}{\sin(\theta + \theta_{bw}(d))} \\ l_3 = \sqrt{l_1^2 + l_2^2 - 2l_1 l_2 \cos(\theta_{bw}(d))} \\ h = (d - l_1)\sin(\theta) \end{cases}$$

$$A_5' \begin{cases} l_1 = \dfrac{l+x}{-cos(\theta)}, \quad l_2 = \dfrac{l+x}{-\cos(\theta + \theta_{bw}(d))} \\ l_3 = \sqrt{l_1^2 + l_2^2 - 2l_1 l_2 \cos(\theta_{bw}(d))} \\ h = (d - l_1)(-\cos(\theta)) \end{cases}$$

$$A_7' \begin{cases} l_1 = \dfrac{l+y}{-\sin(\theta)}, \quad l_2 = \dfrac{l+y}{-\sin(\theta + \theta_{bw}(d))} \\ l_3 = \sqrt{l_1^2 + l_2^2 - 2l_1 l_2 \cos(\theta_{bw}(d))} \\ h = (d - l_1)(-\sin(\theta)) \end{cases}$$

$$A_2' \begin{cases} l_1 = \dfrac{l-y}{\sin(\theta)}, \quad l_2 = \dfrac{l-y}{\sin(\theta + \theta_{bw}(d))} \\ l_3 = \sqrt{l_1^2 + l_2^2 - 2l_1 l_2 \cos(\theta_{bw}(d))} \\ h = (d - l_2)\cos(\theta) \end{cases}$$

$$A_4' \begin{cases} l_1 = \dfrac{l+x}{-\cos(\theta)}, \quad l_2 = \dfrac{l+x}{-\cos(\theta + \theta_{bw}(d))} \\ l_3 = \sqrt{l_1^2 + l_2^2 - 2l_1 l_2 \cos(\theta_{bw}(d))} \\ h = (d - l_2)(-\cos(\theta)) \end{cases}$$

$$A_6' \begin{cases} l_1 = \dfrac{l+y}{-\sin(\theta)}, \quad l_2 = \dfrac{l+y}{-\sin(\theta + \theta_{bw}(d))} \\ l_3 = \sqrt{l_1^2 + l_2^2 - 2l_1 l_2 \cos(\theta_{bw}(d))} \\ h = (d - l_2)(-\sin(\theta)) \end{cases}$$

$$A_8' \begin{cases} l_1 = \dfrac{l-x}{\cos(\theta)}, \quad l_2 = \dfrac{l-x}{\cos(\theta + \theta_{bw}(d))} \\ l_3 = \sqrt{l_1^2 + l_2^2 - 2l_1 l_2 \cos(\theta_{bw}(d))} \\ h = (d - l_2)\cos(\theta) \end{cases}$$

REFERENCES

[1] Q. Xia and J. M. Jornet, "Leveraging antenna side-lobe information for expedited neighbor discovery in directional terahertz communication networks," in *Proc. IEEE 87th Veh. Technol. Conf.*, 2018, pp. 1–6.

[2] Cisco, "Cisco Visual Networking Index: Global mobile data traffic forecast update, 2016–2021," San Jose, CA, USA, White Paper, Jun. 6, 2017.

[3] I. F. Akyildiz, J. M. Jornet, and C. Han, "Terahertz band: Next frontier for wireless communications," *Phys. Commun.*, vol. 12, pp. 16–32, 2014.

[4] T. Kurner and S. Priebe, "Towards THz communications-status in research, standardization and regulation," *J. Infrared, Millimeter, Terahertz Waves*, vol. 35, no. 1, pp. 53–62, 2014.

[5] J. M. Jornet and I. F. Akyildiz, "Channel modeling and capacity analysis of electromagnetic wireless nanonetworks in the terahertz band," *IEEE Trans. Wireless Commun.*, vol. 10, no. 10, pp. 3211–3221, Oct. 2011.

[6] S. Priebe and T. Kurner, "Stochastic modeling of THz indoor radio channels," *IEEE Trans. Wireless Commun.*, vol. 12, no. 9, pp. 4445–4455, Sep. 2013.

[7] J. M. Jornet and I. F. Akyildiz, "Femtosecond-long pulse-based modulation for terahertz band communication in nanonetworks," *IEEE Trans. Commun.*, vol. 62, no. 5, pp. 1742–1754, May 2014.

[8] V. Radisic *et al.*, "Sub-millimeter wave InP technologies and integration techniques," in *Proc. IEEE MTT-S Int. Microw. Symp.*, 2015, pp. 1–4.

[9] S. Slivken and M. Razeghi, "High power, electrically tunable quantum cascade lasers," *Proc. SPIE*, vol. 9755, 2016, Art. no. 97550C.

[10] T. Nitsche, A. B. Flores, E. W. Knightly, and J. Widmer, "Steering with eyes closed: Mm-wave beam steering without in-band measurement," in *Proc. IEEE Conf. Comput. Commun.*, 2015, pp. 2416–2424.

[11] X.-W. Yao and J. M. Jornet, "TAB-MAC: Assisted beamforming MAC protocol for terahertz communication networks," *Nano Commun. Netw.*, vol. 9, pp. 36–42, 2016.

[12] F. Yildirim and H. Liu, "A cross-layer neighbor-discovery algorithm for directional 60-GHz networks," *IEEE Trans. Veh. Technol.*, vol. 58, no. 8, pp. 4598–4604, Oct. 2009.

[13] J. Wang, "Beam codebook based beamforming protocol for multi-Gbps millimeter-wave WPAN systems," *IEEE J. Sel. Areas Commun.*, vol. 27, no. 8, pp. 1390–1399, Oct. 2009.

[14] *IEEE Standard for Information Technology-Telecommunications and Information Exchange Between Systems Local and Metropolitan Area Networks—Specific Requirements—Part 11: Wireless LAN Medium Access Control (MAC) and Physical Layer (PHY) Specifications Amendment 3: Enhancements for Very High Throughput in the 60 GHz Band*, IEEE Standard 802.11.ad-2012 (Amendment to IEEE Std. 802.11.ad-2012), Dec. 28, 2012.

[15] *IEEE Standard for Information Technology- Local and Metropolitan Area Networks—Specific Requirements—Part 15.3: Amendment 2: Millimeter-Wave-Based Alternative Physical Layer Extension*, IEEE Standard 802.15.3c-2009 (Amendment to IEEE Std. 802.15.3-2003), 2009, pp. 1–200.

[16] A. Patra, L. Simi, and M. Petrova, "Experimental evaluation of a novel fast beamsteering algorithm for link re-establishment in mm-wave indoor WLANs," in *Proc. IEEE 27th Annu. Int. Symp. Personal, Indoor, Mobile Radio Commun.*, 2016, pp. 1–7.

[17] G. M. Olcer, Z. Genc, and E. Onur, "Sector scanning attempts for non-isolation in directional 60 GHz networks," *IEEE Commun. Lett.*, vol. 14, no. 9, pp. 845–847, Sep. 2010.

[18] R. Ramanathan, J. Redi, C. Santivanez, D. Wiggins, and S. Polit, "Ad hoc networking with directional antennas: A complete system solution," *IEEE J. Sel. Areas Commun.*, vol. 23, no. 3, pp. 496–506, Mar. 2005.

[19] Y. M. Tsang, A. S. Y. Poon, and S. Addepalli, "Coding the beams: Improving beamforming training in mmwave communication system," in *Proc. IEEE Global Telecommun. Conf.*, 2011, pp. 1–6.

[20] S. K. Saha *et al.*, "X60: A programmable testbed for wideband 60GHz wlans with phased arrays," *Comput. Commun.*, vol. 133, pp. 77–88, 2019.

[21] C. A. Balanis, *Antenna Theory: Analysis and Design*. Hoboken, NJ, USA: Wiley, 2005.

[22] V. Petrov, M. Komarov, D. Moltchanov, J. M. Jornet, and Y. Koucheryavy, "Interference and SINR in millimeter wave and terahertz communication systems with blocking and directional antennas," *IEEE Trans. Wireless Commun.*, vol. 16, no. 3, pp. 1791–1808, Mar. 2017.

[23] S. K. Saha *et al.*, "X60: A programmable testbed for wideband 60GHz wlans with phased arrays," *Comput. Commun.*, vol. 133, pp. 77–88, Jan. 2019.

[24] Q. Xia and J. M. Jornet, "Cross-layer analysis of optimal relaying strategies for terahertz-band communication networks," in *Proc. IEEE 13th Int. Conf. Wireless Mobile Comput., Netw. Commun.*, 2017, pp. 1–8.

Qing Xia received the B.S. degree in electrical engineering from the Hebei University of Technology, Tianjin, China, and the M.S. degree in electrical engineering from the University of Denver, Denver, CO, USA, in 2010 and 2012, respectively. She is currently working toward the Ph.D. degree at the Department of Electrical Engineering, University at Buffalo, The State University of New York, Buffalo, NY, USA. She is currently working as a Graduate Research Assistant under the guidance of Professor Josep Miquel Jornet. She was an intern with Intel Lab, Aloha, OR, USA, in 2016. Her current research interests include Terahertz-band communication networks, nano networks, protocol design, network simulation, and Internet of Things (IoT).

Josep Miquel Jornet received the B.S. degree in telecommunication engineering, the M.Sc. degree in information and communication technologies from the Universitat Politecnica de Catalunya, Barcelona, Spain, in 2008, and the Ph.D. degree in electrical and computer engineering from the Georgia Institute of Technology (Georgia Tech), Atlanta, GA, USA, in 2013. He is currently an Associate Professor with the Department of Electrical Engineering, University at Buffalo (UB), The State University of New York (SUNY), Buffalo, NY, USA. From September 2007 to December 2008, he was a Visiting Researcher with the Massachusetts Institute of Technology (MIT), Cambridge, under the MIT Sea Grant Program. His current research interests include terahertz-band communication networks, nanophotonic wireless communication, wireless nano-bio-sensing networks and the Internet of Nano-Things. In these areas, he has coauthored more than 100 peer-reviewed scientific publications, one book, and has also been granted three U.S. patents. Since July 2016, he is the Editor-in-Chief of *the Nano Communication Networks* (Elsevier) Journal. He is serving as the Lead PI on multiple grants from U.S. federal agencies including the National Science Foundation, the Air Force Office of Scientific Research, and the the Air Force Research Laboratory. He is a recipient of the National Science Foundation CAREER Award and of several other awards from IEEE, ACM as well as UB.